14-3-3ε UFMylation promotes RIG-I-mediated signaling

Isaura Vanessa Gutierrez[1], Moonhee Park[1], Lauren Sar[1], Ryan Rodriguez[2], Daltry L. Snider[2], Gabriella Torres[1], K. Matthew Scaglione[2,3], Stacy M. Horner[1,2,4]

[1] Department of Integrative Immunobiology, Duke University School of Medicine, Durham, NC, USA

[2] Department of Molecular Genetics and Microbiology, Duke University School of Medicine, Durham, NC, USA

[3] Duke Center for Neurodegeneration and Neurotherapeutics, Duke University School of Medicine, Durham, NC, USA

[4] Department of Medicine, Duke University School of Medicine, Durham, NC, USA

Correspondence: stacy.horner@duke.edu
Stacy M. Horner, Ph.D.
Duke University School of Medicine
213 Research Dr., Box 3053 DUMC
Durham, NC USA 27710
Phone: 919-684-1921

Abstract

Post-translational modifications are critical for regulating the RIG-I signaling pathway. Previously, we identified a role for the post-translation modification UFM1 (UFMylation) in promoting RIG-I signaling by stimulating the interaction between RIG-I and its membrane-targeting protein 14-3-3ε. Here, we identify UFMylation of 14-3-3ε as a novel regulatory mechanism promoting RIG-I signaling. We demonstrate that UFM1 conjugation to lysine residue K50 or K215 results in mono-UFMylation on 14-3-3ε and enhances its ability to promote RIG-I signaling. Importantly, we show that mutation of these residues (K50R/K215R) abolishes UFMylation and impairs induction of type I and III interferons without disrupting the interaction between 14-3-3ε and RIG-I. This suggests that UFMylation of 14-3-3ε likely stabilizes signaling events downstream of RIG-I activation to promote induction of interferon. Collectively, our work suggests that UFMylation-driven activation of 14-3-3ε facilitates innate immune signaling and highlights the broader role of UFMylation for antiviral defense and immune regulation.

Importance

Post-translational modifications provide regulatory control of antiviral innate immune responses. Our study reveals that UFMylation of 14-3-3ε is a control point for RIG-I-mediated antiviral signaling. We demonstrate that conjugation of UFM1 to specific lysine residues on 14-3-3ε enhances downstream signaling events that facilitate interferon induction, but surprisingly it does not affect 14-3-3ε binding to RIG-I. By identifying the precise sites of UFMylation on 14-3-3ε and their functional consequences, we provide insights into the regulatory layers governing antiviral innate immunity. These findings complement emerging evidence that UFMylation serves as a versatile modulator across diverse immune pathways. Furthermore, our work highlights how protein chaperones like 14-3-3ε can be dynamically modified to orchestrate complex signaling cascades, suggesting potential therapeutic approaches for targeting dysregulated innate immunity.

Introduction

The antiviral innate immune response is tightly regulated to ensure effective defense against viral infections while preventing excessive inflammation. This antiviral response to RNA viruses is activated by cytosolic RIG-I-like receptors (RLRs) RIG-I and MDA5, which detect pathogen-associated molecular patterns from RNA viruses and initiate the formation of a MAVS-signaling complex (1). This complex activates a downstream signaling cascade that leads to the transcriptional activation of type I and type III interferons (IFN) and the production of IFN-stimulated genes (ISGs) that limit viral replication. Robust innate immune signaling is essential for effective adaptive immunity, but dysregulation of these pathways can result in autoimmune diseases and interferonopathies (2-4). Therefore, the induction of IFN is carefully regulated by mechanisms that temporarily activate, dampen, and ultimately shut down the signaling pathway.

Both 14-3-3ε and 14-3-3η are examples of RLR regulatory proteins that regulate IFN induction. These proteins facilitate the translocation of RIG-I and MDA5, respectively, from the cytosol to intracellular membrane signaling sites to interact with MAVS (5, 6). 14-3-3 proteins are highly conserved regulatory molecules involved in diverse cellular processes, including signal transduction, apoptosis, and stress responses. Typically, they regulate cellular processes by binding to phosphorylated client proteins, although they are also known to bind to non-phosphorylated client proteins, including those containing other post-translational modifications (PTMs) beyond phosphorylation (7-13). Recent work has also suggested that 14-3-3 proteins can serve as protein chaperones, preventing aggregation and phase separation of their client proteins (14). Orthoflavivirus NS3 proteins specifically target and inactivate both 14-3-3ε and 14-3-3η to prevent RLR signaling, and the enterovirus 3C protease cleaves 14-3-3ε, underscoring the essential role of these membrane-targeting proteins in antiviral innate immunity (15-17).

Post-translational modifications play a crucial role in regulating RIG-I signaling (18, 19). Recent studies by our group have shown that ubiquitin-fold modifier 1 (UFM1) and the proteins involved in UFM1 conjugation promote RIG-I signaling (20). UFMylation involves the covalent conjugation of ubiquitin-fold modifier 1 (UFM1), an 85-amino acid peptide, to lysine residues on proteins, utilizing an E1 activating enzyme (UBA5), an E2 conjugating enzyme (UFC1), and an E3 scaffold-like ligase complex (UFL1 and the membrane-anchored protein UFBP1) (21-29). UFM1 is a non-degradative mark, and its addition to proteins can alter their interactions. UFMylation modulates various cellular processes, including the DNA damage response and genomic instability, various aspects of ER homeostasis and translation, ER-Golgi transport, viral infection, cancer progression, and both adaptive and innate immune responses (23, 24, 26, 27, 30-43). For example, UFMylation of the ribosomal protein RPL26 enhances hepatitis A virus

translation (44). In orthoflaviviruses, UFMylation promotes the production of infectious virions (45). Interestingly, viruses have evolved mechanisms to manipulate host UFMylation pathways by targeting UFL1 to specific substrates. For example, orthoflaviviruses co-opt UFL1 to aid in viral assembly (45), while Epstein-Barr virus (EBV) targets UFL1 to MAVS for UFMylation to dampen inflammasome activation (46). Others have shown that UFMylation promotes NLRP3 activation or that it can limit LPS-mediated inflammation via its roles in regulating ER homeostasis and the unfolded protein response (47-51). UFL1 can also bind STING during HSV-1 infection to maintain IFN induction (52). Thus, UFL1 or UFMylation can influence viral infection and innate immune responses in diverse ways.

Our previous work on UFMylation in the context of RIG-I signaling revealed that UFL1 translocates to intracellular membranes upon RIG-I activation (20, 53). We identified roles for UFL1 and UFM1 in facilitating RIG-I interaction with 14-3-3ε and found that 14-3-3ε exhibits increased UFMylation in response to RIG-I activation. However, several critical questions remained unanswered. First, does UFMylation directly modulate 14-3-3ε function during RIG-I signaling? Second, which specific lysine residues on 14-3-3ε serve as UFMylation sites? Third, how does UFMylation functionally impact 14-3-3ε's role in RIG-I-mediated signaling? We hypothesized that direct UFMylation of 14-3-3ε at specific lysine residues enhances its ability to promote RIG-I signaling. Here, we demonstrate that UFM1 conjugation enhances 14-3-3ε-mediated RIG-I signaling. We then identify lysine residues on 14-3-3ε that are UFMylated. Then, we show how UFMylation of these lysine residues regulates RIG-I-dependent IFN induction

Results

UFM1 conjugation is required to promote 14-3-3ε-mediated enhancement of RIG-I signaling to IFN-β. To determine whether UFM1 plays a functional role in enhancing RIG-I signaling through 14-3-3ε, we first assessed its effect on IFN-β promoter activation**.** Using IFN-β promoter luciferase assays in 293T cells, we found that ectopic expression of UFM1 significantly enhanced RIG-I driven signaling to IFN-β. This signaling was further amplified when UFM1 was co-expressed with both RIG-I and 14-3-3ε, suggesting these three proteins cooperate for signaling regulation (Figure 1A). Next, to determine whether the conjugation of UFM1 is specifically required for this enhancement, we generated a conjugation-deficient UFM1 mutant (ΔC3) by deleting three amino acids from its C-terminus to prevent covalent attachment of UFM1 to target proteins (21). Using IFN-β promoter luciferase assays in 293T cells, we found that unlike wild-type UFM1, the conjugation-deficient UFM1 mutant failed to enhance 14-3-3ε-driven RIG-I

116 signaling (Figure 1B). These results demonstrate that UFM1 must be covalently conjugated to
117 proteins to facilitate 14-3-3ε-mediated enhancement of RIG-I signaling to the IFN-β promoter.
118
119 **UFM1 conjugation to 14-3-3ε requires residues K50 and K215 on 14-3-3ε.** Having established
120 that UFM1 conjugation is required for 14-3-3ε-mediated enhancement of RIG-I signaling, we next
121 sought to verify our previous results that 14-3-3ε is directly UFMylated (20) and determine which
122 specific lysine residues serve as UFM1-conjugation sites. First, we wanted to verify 14-3-3ε
123 UFMylation in cells. For this, we developed a modified UFMylation assay based on previous
124 studies (54). In this assay, we co-expressed HA-tagged 14-3-3ε, Flag-UFM1, and the UFMylation
125 ligase complex proteins UFL1 and UFBP1 in 293T-UFM1 KO cells generated by CRISPR/Cas9
126 targeting. Critically, lysates were boiled prior to immunoprecipitation to denature protein
127 complexes, ensuring that only proteins covalently linked to the immunoprecipitated protein would
128 be detected in subsequent analyses. Following HA-immunoprecipitation, we identified a single
129 Flag-UFM1 conjugation to 14-3-3ε, consistent with a mono-UFMylation event (Figure 2A).
130 Importantly, the conjugation-deficient Flag-UFM1-ΔC3 showed no attachment of 14-3-3ε, while a
131 deconjugation-resistant Flag-UFM1-G83A mutant (21) demonstrated significantly increased
132 levels of 14-3-3ε UFMylation.
133 Having established that UFM1 conjugation is required for RIG-I signaling, we next sought
134 to identify the specific lysine residues on 14-3-3ε that undergo UFMylation by using mass
135 spectrometry analysis. We used Huh7 cells stably expressing Flag-UFM1 with a two amino acid
136 deletion (ΔC2) that enhances detection of UFMylated proteins by eliminating the prerequisite of
137 G-SC cleavage in UFM1 by the UFSP1/UFSP2 proteins that needs to occur to initiate the
138 UFMylation pathway (21). After HA-immunoprecipitation of HA-tagged 14-3-3ε, mass
139 spectrometry analysis identified three peptides containing two lysine residues, K50 and K215,
140 that were covalently modified by UFM1. Both K50 and K215 reside within clusters of basic
141 residues within a positively charged pocket of the conserved amphipathic ligand binding groove
142 of 14-3-3 proteins.
143 To confirm these specific sites as bona fide UFMylation targets, we employed both *in vitro*
144 and cellular UFMylation assays. Using an *in vitro* UFMylation assay with purified UFMylation
145 proteins, we demonstrated that wild-type 14-3-3ε has mono-UFMylation, whereas lysine-to-
146 arginine mutations at K50 and K215 (K50R/K215R) abolished this mono-UFMylation (Figure 2B).
147 Similarly, in our cellular UFMylation assay, the K50R-K215R mutations significantly abrogated
148 14-3-3ε mono-UFMylation (Figure 2C). These complementary approaches confirm that K50 and
149 K215 are the principal sites for UFM1 conjugation to 14-3-3ε. However, as we only detect mono-

150 UFMylation of 14-3-3ε, these results also suggest that either K50 or K215 undergo UFM1-
151 conjugation in a molecule of 14-3-3ε.
152
153 **K50 and K215 are not required for 14-3-3ε interaction with RIG-I.** Based on our previous
154 findings that both UFM1 and UFL1 are important for the interaction of RIG-I with 14-3-3ε (20), we
155 hypothesized that UFMylation of 14-3-3ε at either K50 or K215 would be required for its interaction
156 with RIG-I. To test this hypothesis, we performed co-immunoprecipitation experiments comparing
157 RIG-I binding between 14-3-3ε^{WT} or the UFMylation-deficient 14-3-3ε$^{K50/215R}$ mutant.
158 Unexpectedly, we found that 14-3-3ε$^{K50/215R}$ maintained interaction with RIG-I at levels
159 comparable to the wild-type protein (Figure 3A-B), indicating that UFMylation at these residues is
160 not essential for the association of 14-3-3ε and RIG-I. To validate our experimental approach, we
161 included a control mutant of 14-3-3ε where key residues in the C-terminal end (EDE to AAA) were
162 altered, as these previously have been reported to mediate this interaction (55). As expected, this
163 control mutant showed significantly reduced RIG-I binding, confirming the work of others and the
164 specificity of our assay. These results revealed that UFMylation at K50 or K215 are not critical for
165 the interaction between 14-3-3ε and RIG-I.
166
167 **K50 and K215 are required for 14-3-3ε-mediated RIG-I activation of IFN.** Since UFMylation
168 did not affect the binding of for 14-3-3ε to RIG-I, we next investigated whether the K50/K215
169 residues nevertheless impact the ability of 14-3-3ε to enhance RIG-I-mediated signaling using
170 two complementary approaches. First, we evaluated IFN-β promoter activation using a luciferase
171 reporter assay in 293T-RIG-I KO cells. We ectopically expressed 14-3-3ε^{WT} or 14-3-3ε$^{K50/215R}$,
172 along with RIG-I, and measured luciferase activity. While 14-3-3ε^{WT} significantly increased RIG-I
173 signaling to the IFN-β promoter as expected, 14-3-3ε$^{K50/215R}$ showed significantly impaired ability
174 to enhance this signaling (Figure 4A). This result suggests that UFMylation at K50 or K215 is
175 critical for 14-3-3ε to promote RIG-I-mediated transcriptional activation. To directly confirm this
176 finding at the transcriptional level, we measured the induction of endogenous IFN genes by RT-
177 qPCR in response to infection by Sendai virus, a potent activator of RIG-I signaling (56, 57). We
178 ectopically expressed 14-3-3ε^{WT} or 14-3-3ε$^{K50/215R}$, along with RIG-I in 293T-RIG-I KO cells and
179 analyzed the levels of *IFNB1* and *IFNL1* transcripts. Consistent with our luciferase assay results,
180 14-3-3ε$^{K50/215R}$ significantly limited RIG-I-mediated induction of both *IFNB1* and *IFNL1* compared
181 to 14-3-3ε^{WT} (Figure 4B-C). Collectively, these findings demonstrate that while lysine residues
182 required for 14-3-3ε UFMylation do not affect RIG-I binding, they are nevertheless critical for
183 promoting RIG-I-mediated transcriptional activation of type I and type III IFNs, suggesting that

184 UFMylation of 14-3-3ε at K50 and K215 enhances downstream signaling events following initial
185 RIG-I binding.
186
187 **Discussion.**
188 Our study identifies UFMylation of 14-3-3ε as a novel regulatory mechanism that promotes
189 RIG-I-mediated antiviral signaling. Through a series of biochemical and functional analyses, we
190 have demonstrated that UFM1 is covalently conjugated to lysine residues K50 or K215 on 14-3-
191 3ε, and that this modification is critical for 14-3-3ε to enhance RIG-I-dependent IFN induction.
192 Upon viral RNA recognition, activated RIG-I must translocate from the cytosol to intracellular
193 membranes to interact with MAVS within a specialized signaling complex termed the "RIG-I
194 translocon," which includes the K63 ubiquitin ligases TRIM25 and Riplet. One of our most
195 intriguing findings was that mutation of the UFMylation sites (K50R/K215R) abolished the ability
196 of 14-3-3ε to enhance RIG-I signaling without disrupting their physical interaction. This
197 unexpected result suggests that UFMylation modulates 14-3-3ε function through mechanisms
198 beyond simple binding affinity regulation.
199 Previously, we demonstrated that the UFMylation E3 ligase complex member UFL1 is
200 recruited to ER-mitochondrial contact sites following RIG-I activation (20, 53). Our current work
201 extends this model by identifying UFMylation sites on 14-3-3ε (K50 and K215) that are critical for
202 its function in this pathway. The mechanism by which UFMylation enhances 14-3-3ε function may
203 involve electrostatic or conformational changes within its ligand-binding groove as the negative
204 charge of UFM1 in the presence of these positively charged residues is likely to influence how
205 14-3-3ε interacts with and coordinates protein partners at membrane signaling sites (14).
206 Interestingly, our results suggest that only mono-UFMylation occurs on 14-3-3ε. As K50 and K215
207 can reside on opposite faces within the conserved amphipathic ligand-binding groove of 14-3-3ε
208 when 14-3-3ε binds non-phosphorylated proteins, it seems possible that only one site can be
209 UFMylated on any given molecule (10). While the exact function of UFM1-conjugation on 14-3-
210 3ε is still unclear, it may play a role in coordinating multiple protein partners at membrane signaling
211 sites, potentially including known interactors such as Riplet, TRIM25, or MAVS, whose binding to
212 14-3-3ε might be modulated by its UFMylation status. This model aligns with observations in other
213 systems where UFMylation has been shown to serve as a scaffold for optimizing signaling
214 complex organization (40), suggesting a similar role in RIG-I signaling.
215 Our results highlight the sophisticated regulation of 14-3-3 proteins through various PTMs.
216 Interestingly, K50 on 14-3-3ε can be acetylated and sumoylated (58, 59), and this residue in other
217 14-3-3 proteins has been shown to be ubiquitinated (8). This suggests that competing PTMs at

218 the same residue could mediate context-dependent functional switching between distinct cellular
219 pathways. Recent studies have also revealed intrinsic chaperone-like activities for 14-3-3 proteins
220 that broadly prevent aggregation or aberrant phase separation of client proteins (14). We
221 speculate that UFMylation could also enhance these intrinsic chaperone functions of 14-3-3
222 proteins during antiviral responses by stabilizing protein complexes critical to innate immune
223 signaling. This could explain how UFMylation promotes RIG-I signaling without affecting direct
224 binding interactions, by optimizing the molecular environment around the signaling complex
225 rather than altering binding interfaces directly. Future studies will be needed to investigate the
226 molecular events triggering site-specific UFMylation of 14-3-3 following RIG-I activation and to
227 determine whether other 14-3-3 isoforms undergo similar regulation.
228 In summary, by identifying K50 and K215 on 14-3-3ε as a critical target residues of
229 UFMylation that promote RIG-I signaling, our study reveals another mechanism for how this post-
230 translational modification system tunes diverse innate immune pathways, advancing our
231 fundamental understanding of innate immune regulation. The UFMylation pathway represents a
232 potential target for modulating antiviral responses in conditions characterized by either insufficient
233 immunity or excessive inflammation. Furthermore, as viruses have evolved mechanisms to
234 manipulate UFMylation, targeting this pathway could potentially disrupt various aspects of viral
235 infection. Future investigations of UFMylation in both infectious and inflammatory diseases may
236 yield important insights for developing novel immunomodulatory approaches.
237
238 **Acknowledgements**
239 We thank those colleagues who generously provided reagents, as indicated in the Methods, the
240 Duke Functional Genomics Core, the Duke Proteomics and Metabolomics Core Facility, and
241 members of the Horner Lab for valuable feedback and discussion. This work was supported by
242 National Institutes of Health grants R01AI155512 (S.M.H), R35GM119544 (K.M.S), and
243 T32CA00911 (IVG; DLS).
244

245 **Figures**

246

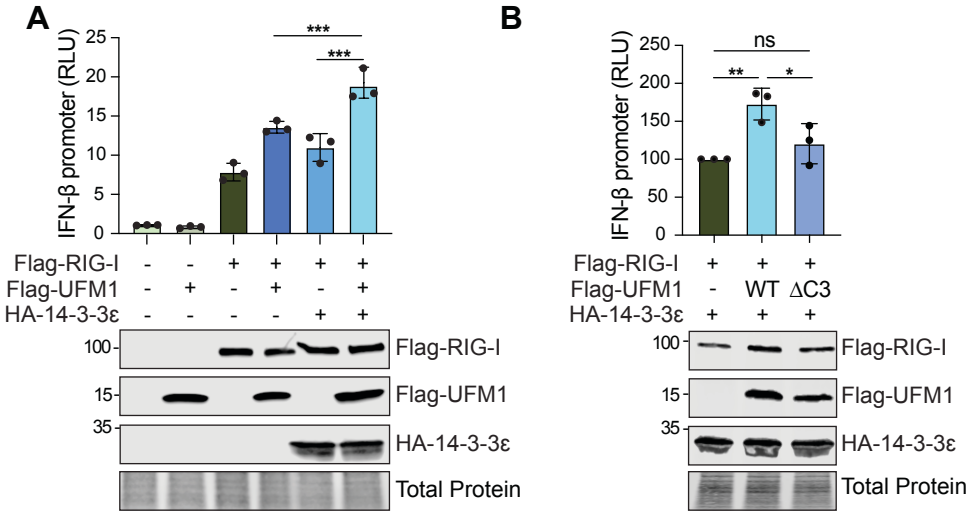

247

248

249 **Figure 1. UFM1 conjugation is required to promote 14-3-3ε-mediated enhancement of RIG-**
250 **I signaling to IFN-β.** (A) IFN-β-promoter reporter luciferase expression (relative to *Renilla)* from
251 293T cells expressing (Vec) Vector, Flag-UFM1^{WT}, Flag-RIG-I, or HA-14-3-3ε. (B) IFN-β–
252 promoter reporter luciferase expression (relative to *Renilla*) from 293T cells expressing (Vec)
253 Vector, Flag-UFM1^{WT}, Flag-UFM1$^{\Delta C3}$, Flag-RIG-I, or HA-14-3-3ε. Bars represent the mean ± SD,
254 $n = 3$ independent replicates. *p ≤ 0.05, ** ≤ 0.01, ***p ≤ 0.001 determined by one way ANOVA
255 followed by Šidák's multiple comparisons test (A) or Tukey's multiple comparisons test (B).

256

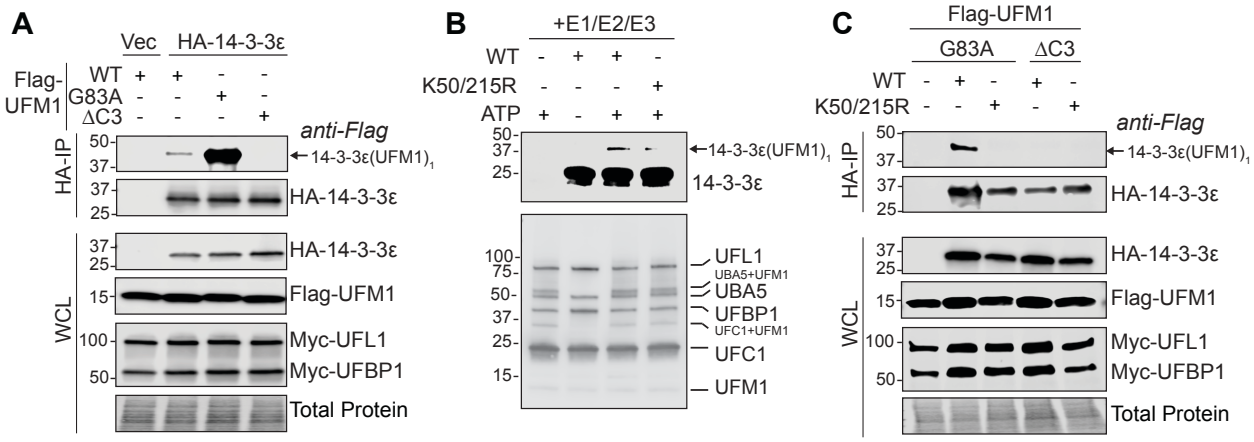

Figure 2. UFM1 conjugation to 14-3-3ε requires residues K50 and K215 on 14-3-3ε. (A) UFMylation assay of anti-HA immunoprecipitated lysates from 293T UFM1 KO cells expressing Vector (Vec) or HA-14-3-3ε along with Myc-UFL1, Myc-UFBP1, and Flag-UFM1-WT, -G83A, or -ΔC3. (B) Purified UFMylation proteins (UFBP1, UFL1, UFC1, UBA5, and UFM1) as well as 14-3-3ε^{WT} or 14-3-3ε$^{K50/215R}$ were incubated in UFMylation assay buffer in the presence or absence of ATP. Following reaction termination, the samples were subjected to immunoblot analysis for 14-3-3ε (top) or using an antibody cocktail to all UFMylation proteins (bottom). (C) UFMylation assay of anti-HA immunoprecipitated lysates from 293T UFM1 KO cells expressing Vector (-), Flag-UFM1-WT, -G83A, or -ΔC3, and HA-14-3-3ε^{WT} or HA-14-3-3ε$^{K50/215R}$. Representative blots from $n = 3$ independent replicates are shown.

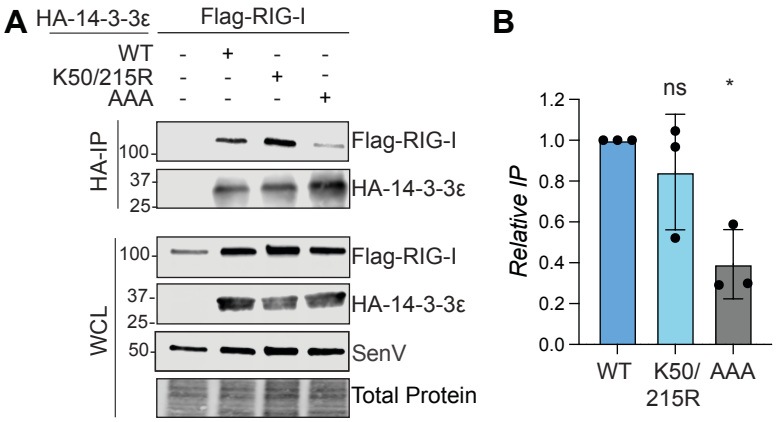

Figure 3. K50 and K215 are not required for 14-3-3ε interaction with RIG-I. (A) Immunoblot analysis of anti-HA immunoprecipitated extracts and inputs from 293T RIG-I KO cells expressing Flag-RIG-I, and HA-14-3-3ε WT, K50/215R, or AAA. Representative blot from $n = 3$ independent replicates is shown. (B) Relative quantification of the ratio of RIG-I (IP/relative input) to immunoprecipitated 14-3-3ε is shown on the right (Mean ± SD, $n = 3$). *$p \leq 0.05$ or non-significant (ns) determined by one way ANOVA followed by Tukey's multiple comparisons test.

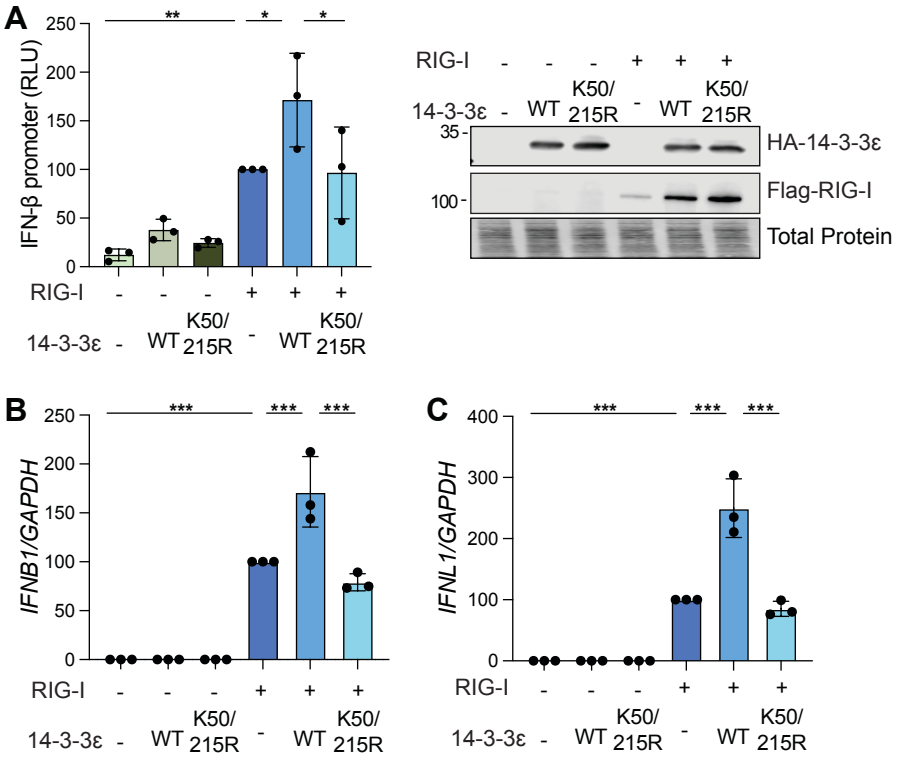

Figure 4. K50 and K215 are required for 14-3-3ε-mediated RIG-I activation of IFN. (A) IFN-β-promoter reporter luciferase expression from 293T RIG-I KO cells expressing Vector (-), Flag-RIG-I, and HA-14-3-3ε^{WT} or HA-14-3-3ε$^{K50/215R}$, with RIG-I samples normalized to 100. (B-C) RT-qPCR analysis (rel. to *GAPDH*) of RNA extracted from 293T RIG-I KO cells transfected with Flag-RIG-I, and HA-14-3-3ε^{WT} or HA-14-3-3ε$^{K50/215R}$ followed by Sendia virus infection (6 h), with RIG-I samples normalized to 100. *p ≤ 0.05, ** ≤ 0.01, ***p ≤ 0.005 determined by one way ANOVA followed by (A) Bonferroni or (B-C) Tukey's multiple comparisons test. Mean ± SD, n = 3 independent replicates are shown.

295 **Methods**

296 **Cell lines, viruses, and transfection.** 293T, 293T-UFM1 KO, and 293T-RIG-I KO were grown
297 in Dulbecco's modification of Eagle's medium (DMEM; Mediatech) supplemented with 10% fetal
298 bovine serum, 1X minimum essential medium nonessential amino acids, and 25 mM of HEPES
299 buffer. The 293T cells (CRL-3216) were obtained from American Type Culture Collection (ATCC).
300 293T-UFM1 KO and 293T-RIG-I KO were previously described (20, 60). All cell lines were verified
301 as mycoplasma-free using the Look-Out Mycoplasma PCR detection kit (Sigma-Aldrich). Sendai
302 virus Cantell strain was obtained from Charles River Laboratories and used at 200 HAU/ml.
303 Sendai virus infections were performed in serum-free media (30 to 60 mins), after which complete
304 medium was added. DNA transfections were performed using FuGene 6 (Promega). Cells were
305 incubated for 24-48 hours post transfection prior to experimental treatment.

306

307 **Plasmids.** The following plasmids have been previously described: pIFN-β-luc (61), pCMV-
308 Renilla (Promega), pcTak_Myc-5_UFL1 (20), pETDuet-His$_6$-TEV-UFL1-StrepII-3C-UFBP1$^{(21\text{-end})}$
309 (gift of Dr. Yogesh Kulathu) (28), pTRIPZ IFNB1^{2x}-Gluc (gift of Dr. Nandan Gokhale) (60), and
310 pET-NT*-HRV3CP (gift of Dr. Gottfried Otting; Addgene #162795) (55). The following plasmids
311 were generated by insertion of PCR-amplified fragments into NotI-to-PmeI digested pEF-TAK-
312 Flag or into BamHI-to-NotI digested pGEX-GST using InFusion cloning (Takara): pGEX-GST-14-
313 3-3ε^{WT}, pGEX-GST-14-3-3ε$^{K50/215R}$, pGEX-GST-UBA5, pGEX-GST-UFC1, and pGEX-GST-
314 UFM1. The following plasmids were generated by site-directed mutagenesis: pEF-TAK-HA-14-3-
315 3ε$^{K50/215R}$, pEF-TAK-HA-14-3-3ε^{AAA} (E251-253A), and pEF-TAK-Flag-UFM1$^{\Delta C2}$. The following
316 were cloned by InFusion: pEF-TAK-Flag-UFM1^{WT}, pEF-TAK-Flag-UFM1$^{\Delta C3}$, and pEF-TAK-Flag-
317 UFM1 G83A from pEF-TAK-HA-UFM1 (20); pEF-TAK-Flag-RIG-I from pEF-Bos-Flag-RIG-I (62),
318 pEF-TAK-HA-14-3-3ε^{WT} from pEF-TAK-Flag-14–3-3ε (20), and pEF-TAK-Myc-UFBP1 by PCR
319 from BC115617. Plasmid sequences were verified by DNA sequencing.

320

321 **IFN-β promoter luciferase assay.** IFN-β promoter luciferase assays were performed at 18 to 24
322 hours after treatment and transfection of pIFN-β-luc and pCMV-Renilla by using the Dual-
323 Luciferase Reporter System (Promega). *Firefly* luciferase was normalized to *Renilla* luciferase,
324 whose expression is driven by the CMV promoter. For the *Gaussia* luciferase assays, 48 hours
325 post transfection of pTRIPZ IFNB1^{2x}-Gluc, supernatant was assayed for *Gaussia* luciferase using
326 the *Renilla* Luciferase Assay System (Promega). All samples were read using a BioTek Synergy2
327 microplate reader.

328

329 **Immunoblotting.** Cells were lysed with either RIPA (10 mM tris HCl pH [7.5], 150 mM NaCl, 0.5%
330 sodium deoxycholate, and 1% Triton X-100 or NP-40 Lysis Buffer (20 mM Tris HCl [pH 7.4], 100
331 mM NaCl, 0.5% NP-40) supplemented with protease inhibitor mixture (Sigma-Aldrich), and Halt
332 inhibitor phosphatase (Thermo Fisher Scientific), and lysates were isolated by centrifugation.
333 Quantified protein was resolved by SDS/PAGE and transferred to nitrocellulose membranes.
334 Membranes were stained with Revert 700 total protein stain (Li-COR Biosciences) and then
335 blocked with 3% bovine serum albumin in phosphate-buffered saline containing 0.01% Tween-
336 20 (PBS-T). Following incubation with primary antibodies, membranes were incubated with
337 species-specific horseradish-peroxidase (HRP)-conjugated antibodies (Jackson Immuno
338 Research 1:5000), followed by membrane treatment with Clarity Western ECL substrate (Bio-
339 Rad) and imaging on a LICOR Odyssey FC. The following antibodies were used for
340 immunoblotting: R-anti-SenV (MBL, 1:1000), HA-HRP (Sigma-Aldrich 1:1000-1:3000), Flag-HRP
341 (1:1000-1:5000), and M-anti-Myc (Cell Signaling Technology 1:1000).
342
343 **Protein immunoprecipitation.** Cells were lysed with either RIPA (10 mM tris HCl [pH 7.5], 150
344 mM NaCl, 0.5% sodium deoxycholate, and 1% triton X-100 or NP-40 Lysis Buffer (20 mM Tris
345 HCl [pH 7.4], 100 mM NaCl, 0.5% NP-40) supplemented with protease inhibitor mixture (Sigma-
346 Aldrich), and Halt phosphatase inhibitor, and 10% glycerol. Quantified protein (between 100-200
347 µg) was incubated anti-HA magnetic beads (Invitrogen) in lysis buffer either at room temperature
348 for 1-2 hrs or 4°C overnight with head-over-tail rotation. Beads were washed 3X in lysis buffer
349 and eluted with 2X Laemmli buffer (Bio-Rad) with 5% 2-mercaptoenthanol at 95°C for 5 minutes.
350 Proteins were resolved by SDS/PAGE and immunoblotting, as above. For UFMylation
351 precipitations, cells were lysed UFMylation lysis buffer (50 mM Tris [pH 8], 150 mM NaCl, 0.5%
352 sodium deoxycholate, and 1% NP-40) supplemented with 10% glycerol, 1:100 protease and
353 phosphatase inhibitors, as above, and 1:100 *N*-ethylmaleimide (10 mM final) (Sigma-Aldrich).
354 Post-nuclear lysates were boiled at 95°C for 10 mins and incubated with Pierce anti-HA magnetic
355 beads with UFMylation lysis buffer. Beads were washed 3X in high salt buffer (10 mM Tris [pH 8],
356 1 mM EDTA, 500 mM NaCl) and eluted with 2X Laemmli buffer with 5% 2-mercaptoenthanol at
357 95°C for 5 minutes.
358
359 **Quantification of immunoblots.** Immunoblots were imaged using the LICOR Odyssey FC
360 system and quantified using ImageStudio software, and raw values were normalized to relevant
361 controls for each antibody. RIG-I and 14-3-3ε interaction were quantified as ratio of inputs of RIG-

362 I and 14-3-3ε normalized to total protein and displayed as the relative ratio of RIG-I over 14-3-3ε
363 pull down.
364
365 **Purification of GST/His-tagged proteins.** pGEX-GST-UBA5, pGEX-GST-UFC1, pGEX-GST-
366 UFM1, pGEX-GST-14-3-3ε, pGEX-GST-14-3-3ε K50/215R, and pETDuet-His_6-TEV-UFL1-
367 StrepII-3C-UFBP1$^{(21\text{-end})}$ were transformed in *E. coli* Rosetta cells. Cells were cultured at 37°C
368 until OD600 reached 0.6 to 0.8. Then, cells were induced with a final concentration of 1 mM IPTG.
369 Cells were further cultured at 30°C for 3.5-4 hours. Cells were collected by centrifugation for 30
370 mins at 7,000 rpm. The pellets were lysed in NET--N buffer (50 mM Tris-HCl [pH 7.5], 150 mM
371 NaCl, 0.5% IGEPAL, supplemented with Aprotinin, Leupeptin, PMSF, and dithiothreitol (DTT) at
372 1:100. Cells were sonicated 3 times for 30 sec at output 6-7 and a duty cycle of 80%. Then,
373 lysates were centrifuged for 30 mins at 12,000 rpm at 4°C. Supernatant was incubated with GST
374 beads that were washed with NETN buffer with rotation at 4C for 1-2 hours. The beads were
375 washed 3 times with NETN buffer and 3 times with PBS supplemented with 1:100 DTT. After
376 washes, GST tag was cleaved with purified human rhinovirus 3C protease (purified as described
377 (55)) and protein was eluted with PBS by incubation with rotation at 4°C overnight.
378
379 ***In vitro* UFMylation.** 2 μM of substrate, 0.25 μM of UBA5, 5 μM UFC1, 20 ng UFL1/UFBP1, 30
380 μM UFM1 were incubated in a reaction buffer containing 50 mM HEPES [pH 7.5], 10 mM $MgCl_2$,
381 with or without 5 mM ATP for 1 hr at 37°C. The reaction was stopped by the addition of 2X SDS
382 loading with 5% 2-mercaptoethanol and incubated at 95°C for 5 minutes The reaction products
383 were then separated by SDS/PAGE and analyzed by immunoblotting, as above.
384
385 **RNA Analysis.** Total cellular RNA was extracted using RNeasy Plus mini kit (Qiagen). RNA was
386 then reverse transcribed using iScript complementary DNA (cDNA) synthesis kit (Bio-Rad),
387 following manufacturer's instructions. The resulting DNA was diluted 1:3 in double distilled water.
388 RT-qPCR was performed in triplicate using the Power SYBR Green PCR master mix (Thermo
389 Fisher Scientific) and QuantStudio 6 Flex RT-PCR system. Oligonucleotide sequences are as
390 follows: IFNB1 F-5'-CTTTGCTATTTTCAGACAAGATTCA; R-5'GCCAGGAGGTTCTCAACAAT,
391 IFNL1 F-5'-CTTCCAAGCCCACCACAACT; R-5'-GGCCTCCAGGACCTTCAGC, and
392 GAPDH F-5'-AAGGTGAAGGTCGGAGTCAAC; R-5'-GGGGTCATTGATGGCAACAATA.
393
394 **Sample Preparation and LC-MS/MS Analysis.** Samples were spiked with undigested bovine
395 casein at a total of either 120 or 240 pmol as an internal quality control standard. Next, samples

396 were supplemented with 10 µL of 20% SDS, reduced with 10 mM DTT for 30 min at 80°C,
397 alkylated with 20 mM iodoacetamide for 30 min at room temperature, then supplemented with a
398 final concentration of 1.2% phosphoric acid and 546 µL of S-Trap (Protifi) binding buffer (90%
399 MeOH/100 mM TEAB). Proteins were trapped on the S-Trap micro cartridge, digested using 20
400 ng/µL sequencing grade trypsin (Promega) for 1 hr at 47°C, and eluted using 50 mM TEAB,
401 followed by 0.2% FA, and lastly using 50% ACN/0.2% FA. All samples were then lyophilized to
402 dryness. Samples were resolubilized using 48 µL of 1% TFA/2% ACN with 25 fmol/µL yeast ADH.
403 Quantitative LC/MS/MS was performed on 1.5 µL (3.13% of total sample) using an MClass UPLC
404 system (Waters Corp) coupled to an Orbitrap Fusion Lumos high resolution accurate mass
405 tandem mass spectrometer (Thermo Fisher Scientific) via a nanoelectrospray ionization source.
406 Briefly, the sample was first trapped on a Symmetry C18 20 mm × 180 µm trapping column (5
407 µl/min at 99.9/0.1 v/v water/acetonitrile), after which, the analytical separation was performed
408 using a 1.8 µm Acquity HSS T3 C18 75 µm × 250 mm column (Waters Corp.) with a 90-min linear
409 gradient of 5 to 30% acetonitrile with 0.1% formic acid at a flow rate of 400 nanoliters/minute
410 (nL/min) with a column temperature of 55°C. Data collection on the Fusion Lumos mass
411 spectrometer was performed in a data-dependent acquisition (DDA) mode of acquisition with a
412 r=120,000 (@ m/z 200) full MS scan from m/z 375 – 1500 with a target AGC value of 4e5 ions
413 was performed. MS/MS scans were acquired in the linear ion trap in “rapid” mode with a target
414 AGC value of 1e5 and max fill time of 100 ms. The total cycle time 2s, with total cycle times of 2
415 sec between like full MS scans. A 20s dynamic exclusion was employed to increase depth of
416 coverage. The total analysis cycle time for each sample injection was approximately 2 hours.
417
418 **Proteomics Data Analysis.** Following UPLC-MS/MS analyses, data were imported into
419 Proteome Discoverer 2.5 (Thermo Fisher Scientific). In addition to quantitative signal extraction,
420 the MS/MS data was searched against the SwissProt *H. sapiens* database (downloaded in Nov
421 2019) and a common contaminant/spiked protein database (bovine albumin, bovine casein, yeast
422 ADH, etc.), and an equal number of reversed-sequence “decoys” for false discovery rate
423 determination. Sequest (v 2.5, Thermo PD) was utilized to produce fragment ion spectra and to
424 perform the database searches. Database search parameters included fixed modification on Cys
425 (carbamidomethyl) and variable modification on Met (oxidation) and Lys (UFMylation). Search
426 tolerances were 2ppm precursor and 0.8Da product ion with semi-trypsin enzyme rules.
427 Discoverer were used to annotate the data at a maximum 1% protein false discovery rate based
428 on q-value calculations. Note that peptide homology was addressed using razor rules in which a
429 peptide matched to multiple different proteins was exclusively assigned to the protein has more

430 identified peptides. Protein homology was addressed by grouping proteins that had the same set
431 of peptides to account for their identification. A master protein within a group was assigned based
432 on % coverage.
433
434 **Statistical analysis.** We used one-way ANOVA followed by appropriate multiple comparisons
435 test using GraphPad Prism software. Graphed values are presented as mean ± SD (n = 3); *$P \leq$
436 0.05, **$P \leq 0.01$, and ***$P \leq 0.001$.
437

438 **References**

439 1. Rehwinkel J, Gack MU. 2020. RIG-I-like receptors: their regulation and roles in RNA
440 sensing. Nat Rev Immunol 20:537-551.

441 2. Crow YJ, Stetson DB. 2022. The type I interferonopathies: 10 years on. Nat Rev
442 Immunol 22:471-483.

443 3. Iwasaki A, Medzhitov R. 2015. Control of adaptive immunity by the innate immune
444 system. Nat Immunol 16:343-53.

445 4. Taft J, Bogunovic D. 2018. The Goldilocks Zone of Type I IFNs: Lessons from Human
446 Genetics. J Immunol 201:3479-3485.

447 5. Lin JP, Fan YK, Liu HM. 2019. The 14-3-3eta chaperone protein promotes antiviral
448 innate immunity via facilitating MDA5 oligomerization and intracellular redistribution.
449 PLoS Pathog 15:e1007582.

450 6. Liu HM, Loo YM, Horner SM, Zornetzer GA, Katze MG, Gale M, Jr. 2012. The
451 mitochondrial targeting chaperone 14-3-3epsilon regulates a RIG-I translocon that
452 mediates membrane association and innate antiviral immunity. Cell Host Microbe
453 11:528-37.

454 7. Aitken A. 2011. Post-translational modification of 14-3-3 isoforms and regulation of
455 cellular function. Semin Cell Dev Biol 22:673-80.

456 8. Pennington KL, Chan TY, Torres MP, Andersen JL. 2018. The dynamic and stress-
457 adaptive signaling hub of 14-3-3: emerging mechanisms of regulation and context-
458 dependent protein-protein interactions. Oncogene 37:5587-5604.

459 9. Henriksson ML, Francis MS, Peden A, Aili M, Stefansson K, Palmer R, Aitken A,
460 Hallberg B. 2002. A nonphosphorylated 14-3-3 binding motif on exoenzyme S that is
461 functional in vivo. Eur J Biochem 269:4921-9.

462 10. Ottmann C, Yasmin L, Weyand M, Veesenmeyer JL, Diaz MH, Palmer RH, Francis MS,
463 Hauser AR, Wittinghofer A, Hallberg B. 2007. Phosphorylation-independent interaction
464 between 14-3-3 and exoenzyme S: from structure to pathogenesis. EMBO J 26:902-13.

465 11. Liu J, Cao S, Ding G, Wang B, Li Y, Zhao Y, Shao Q, Feng J, Liu S, Qin L, Xiao Y. 2021.
466 The role of 14-3-3 proteins in cell signalling pathways and virus infection. J Cell Mol Med
467 25:4173-4182.

468 12. Obsilova V, Obsil T. 2022. Structural insights into the functional roles of 14-3-3 proteins.
469 Front Mol Biosci 9:1016071.

470 13. Toleman CA, Schumacher MA, Yu SH, Zeng W, Cox NJ, Smith TJ, Soderblom EJ,
471 Wands AM, Kohler JJ, Boyce M. 2018. Structural basis of O-GlcNAc recognition by
472 mammalian 14-3-3 proteins. Proc Natl Acad Sci U S A 115:5956-5961.

473 14. Segal D, Maier S, Mastromarco GJ, Qian WW, Nabeel-Shah S, Lee H, Moore G,
474 Lacoste J, Larsen B, Lin ZY, Selvabaskaran A, Liu K, Smibert C, Zhang Z, Greenblatt J,

475 Peng J, Lee HO, Gingras AC, Taipale M. 2023. A central chaperone-like role for 14-3-3
476 proteins in human cells. Mol Cell 83:974-993 e15.

477 15. Chan YK, Gack MU. 2016. A phosphomimetic-based mechanism of dengue virus to
478 antagonize innate immunity. Nat Immunol 17:523-30.

479 16. Riedl W, Acharya D, Lee JH, Liu G, Serman T, Chiang C, Chan YK, Diamond MS, Gack
480 MU. 2019. Zika Virus NS3 Mimics a Cellular 14-3-3-Binding Motif to Antagonize RIG-I-
481 and MDA5-Mediated Innate Immunity. Cell Host Microbe 26:493-503 e6.

482 17. Andrews DDT, Vlok M, Akbari Bani D, Hay BN, Mohamud Y, Foster LJ, Luo H, Overall
483 CM, Jan E. 2023. Cleavage of 14-3-3epsilon by the enteroviral 3C protease dampens
484 RIG-I-mediated antiviral signaling. J Virol 97:e0060423.

485 18. Liu J, Qian C, Cao X. 2016. Post-Translational Modification Control of Innate Immunity.
486 Immunity 45:15-30.

487 19. Zhou Y, He C, Wang L, Ge B. 2017. Post-translational regulation of antiviral innate
488 signaling. Eur J Immunol 47:1414-1426.

489 20. Snider DL, Park M, Murphy KA, Beachboard DC, Horner SM. 2022. Signaling from the
490 RNA sensor RIG-I is regulated by ufmylation. Proc Natl Acad Sci U S A
491 119:e2119531119.

492 21. Komatsu M, Chiba T, Tatsumi K, Iemura S, Tanida I, Okazaki N, Ueno T, Kominami E,
493 Natsume T, Tanaka K. 2004. A novel protein-conjugating system for Ufm1, a ubiquitin-
494 fold modifier. EMBO J 23:1977-86.

495 22. Tatsumi K, Sou YS, Tada N, Nakamura E, Iemura S, Natsume T, Kang SH, Chung CH,
496 Kasahara M, Kominami E, Yamamoto M, Tanaka K, Komatsu M. 2010. A novel type of
497 E3 ligase for the Ufm1 conjugation system. J Biol Chem 285:5417-27.

498 23. Komatsu M, Inada T, Noda NN. 2024. The UFM1 system: Working principles, cellular
499 functions, and pathophysiology. Mol Cell 84:156-169.

500 24. Wei Y, Xu X. 2016. UFMylation: A Unique & Fashionable Modification for Life. Genomics
501 Proteomics Bioinformatics 14:140-146.

502 25. Banerjee S, Kumar M, Wiener R. 2020. Decrypting UFMylation: How Proteins Are
503 Modified with UFM1. Biomolecules 10.

504 26. Millrine D, Peter JJ, Kulathu Y. 2023. A guide to UFMylation, an emerging
505 posttranslational modification. FEBS J 290:5040-5056.

506 27. Zhou X, Mahdizadeh SJ, Le Gallo M, Eriksson LA, Chevet E, Lafont E. 2024.
507 UFMylation: a ubiquitin-like modification. Trends Biochem Sci 49:52-67.

508 28. Peter JJ, Magnussen HM, DaRosa PA, Millrine D, Matthews SP, Lamoliatte F,
509 Sundaramoorthy R, Kopito RR, Kulathu Y. 2022. A non-canonical scaffold-type E3
510 ligase complex mediates protein UFMylation. EMBO J 41:e111015.

511 29. Zhang Y, Yan M, Yu Y, Wang J, Jiao Y, Zheng M, Zhang S. 2024. 14-3-3epsilon: a
512 protein with complex physiology function but promising therapeutic potential in cancer.
513 Cell Commun Signal 22:72.

514 30. Liang Z, Ning R, Wang Z, Kong X, Yan Y, Cai Y, He Z, Liu XG, Zou Y, Zhou J. 2024.
515 The emerging roles of UFMylation in the modulation of immune responses. Clin Transl
516 Med 14:e70019.

517 31. Qin B, Yu J, Nowsheen S, Wang M, Tu X, Liu T, Li H, Wang L, Lou Z. 2019. UFL1
518 promotes histone H4 ufmylation and ATM activation. Nat Commun 10:1242.

519 32. Qin B, Yu J, Nowsheen S, Zhao F, Wang L, Lou Z. 2020. STK38 promotes ATM
520 activation by acting as a reader of histone H4 ufmylation. Sci Adv 6:eaax8214.

521 33. Ishimura R, El-Gowily AH, Noshiro D, Komatsu-Hirota S, Ono Y, Shindo M, Hatta T, Abe
522 M, Uemura T, Lee-Okada HC, Mohamed TM, Yokomizo T, Ueno T, Sakimura K,
523 Natsume T, Sorimachi H, Inada T, Waguri S, Noda NN, Komatsu M. 2022. The UFM1
524 system regulates ER-phagy through the ufmylation of CYB5R3. Nat Commun 13:7857.

525 34. Liang JR, Lingeman E, Luong T, Ahmed S, Muhar M, Nguyen T, Olzmann JA, Corn JE.
526 2020. A Genome-wide ER-phagy Screen Highlights Key Roles of Mitochondrial
527 Metabolism and ER-Resident UFMylation. Cell 180:1160-1177 e20.

528 35. Scavone F, Gumbin SC, Da Rosa PA, Kopito RR. 2023. RPL26/uL24 UFMylation is
529 essential for ribosome-associated quality control at the endoplasmic reticulum. Proc Natl
530 Acad Sci U S A 120:e2220340120.

531 36. Walczak CP, Leto DE, Zhang L, Riepe C, Muller RY, DaRosa PA, Ingolia NT, Elias JE,
532 Kopito RR. 2019. Ribosomal protein RPL26 is the principal target of UFMylation. Proc
533 Natl Acad Sci U S A 116:1299-1308.

534 37. Wang L, Xu Y, Rogers H, Saidi L, Noguchi CT, Li H, Yewdell JW, Guydosh NR, Ye Y.
535 2020. UFMylation of RPL26 links translocation-associated quality control to endoplasmic
536 reticulum protein homeostasis. Cell Res 30:5-20.

537 38. Xu X, Huang W, Bryant CN, Dong Z, Li H, Wu G. 2024. The ufmylation cascade controls
538 COPII recruitment, anterograde transport, and sorting of nascent GPCRs at ER. Sci Adv
539 10:eadm9216.

540 39. He C, Xing X, Chen HY, Gao M, Shi J, Xiang B, Xiao X, Sun Y, Yu H, Xu G, Yao Y, Xie
541 Z, Xing Y, Budiarto BR, Chen SY, Gao Y, Lee YR, Zhang J. 2024. UFL1 ablation in T
542 cells suppresses PD-1 UFMylation to enhance anti-tumor immunity. Mol Cell 84:1120-
543 1138 e8.

544 40. Yoo HM, Kang SH, Kim JY, Lee JE, Seong MW, Lee SW, Ka SH, Sou YS, Komatsu M,
545 Tanaka K, Lee ST, Noh DY, Baek SH, Jeon YJ, Chung CH. 2014. Modification of ASC1
546 by UFM1 is crucial for ERalpha transactivation and breast cancer development. Mol Cell
547 56:261-274.

548 41. Zhou J, Ma X, He X, Chen B, Yuan J, Jin Z, Li L, Wang Z, Xiao Q, Cai Y, Zou Y, Cong
549 YS. 2023. Dysregulation of PD-L1 by UFMylation imparts tumor immune evasion and
550 identified as a potential therapeutic target. Proc Natl Acad Sci U S A 120:e2215732120.

551 42. Lee L, Perez Oliva AB, Martinez-Balsalobre E, Churikov D, Peter J, Rahmouni D, Audoly
552 G, Azzoni V, Audebert S, Camoin L, Mulero V, Cayuela ML, Kulathu Y, Geli V, Lachaud
553 C. 2021. UFMylation of MRE11 is essential for telomere length maintenance and
554 hematopoietic stem cell survival. Sci Adv 7:eabc7371.

555 43. Wang Z, Gong Y, Peng B, Shi R, Fan D, Zhao H, Zhu M, Zhang H, Lou Z, Zhou J, Zhu
556 WG, Cong YS, Xu X. 2019. MRE11 UFMylation promotes ATM activation. Nucleic Acids
557 Res 47:4124-4135.

558 44. Kulsuptrakul J, Wang R, Meyers NL, Ott M, Puschnik AS. 2021. A genome-wide
559 CRISPR screen identifies UFMylation and TRAMP-like complexes as host factors
560 required for hepatitis A virus infection. Cell Rep 34:108859.

561 45. Schmidt HM, Sorensen GC, Lanahan MR, Grabowski J, Park M, Horner SM. 2025.
562 UFMylation promotes orthoflavivirus infectious particle production. bioRxiv
563 doi:10.1101/2025.01.09.632082:2025.01.09.632082.

564 46. Yiu SPT, Zerbe C, Vanderwall D, Huttlin EL, Weekes MP, Gewurz BE. 2023. An
565 Epstein-Barr virus protein interaction map reveals NLRP3 inflammasome evasion via
566 MAVS UFMylation. Mol Cell 83:2367-2386 e15.

567 47. Jing J, Yang F, Wang K, Cui M, Kong N, Wang S, Qiao X, Kong F, Zhao D, Ji J, Tang L,
568 Gao J, Cong YS, Ding D, Chen K. 2025. UFMylation of NLRP3 Prevents Its Autophagic
569 Degradation and Facilitates Inflammasome Activation. Adv Sci (Weinh)
570 doi:10.1002/advs.202406786:e2406786.

571 48. Wang X, Li C, Wang Y, Li L, Han Z, Wang G. 2020. UFL1 Alleviates LPS-Induced
572 Apoptosis by Regulating the NF-kappaB Signaling Pathway in Bovine Ovarian
573 Granulosa Cells. Biomolecules 10.

574 49. Cai Y, Zhu G, Liu S, Pan Z, Quintero M, Poole CJ, Lu C, Zhu H, Islam B, Riggelen JV,
575 Browning D, Liu K, Blumberg R, Singh N, Li H. 2019. Indispensable role of the Ubiquitin-
576 fold modifier 1-specific E3 ligase in maintaining intestinal homeostasis and controlling
577 gut inflammation. Cell Discov 5:7.

578 50. Li C, Li L, Chen K, Wang Y, Yang F, Wang G. 2019. UFL1 Alleviates
579 Lipopolysaccharide-Induced Cell Damage and Inflammation via Regulation of the
580 TLR4/NF-kappaB Pathway in Bovine Mammary Epithelial Cells. Oxid Med Cell Longev
581 2019:6505373.

582 51. Balce DR, Wang YT, McAllaster MR, Dunlap BF, Orvedahl A, Hykes BL, Jr., Droit L,
583 Handley SA, Wilen CB, Doench JG, Orchard RC, Stallings CL, Virgin HW. 2021.
584 UFMylation inhibits the proinflammatory capacity of interferon-gamma-activated
585 macrophages. Proc Natl Acad Sci U S A 118.

586 52. Tao Y, Yin S, Liu Y, Li C, Chen Y, Han D, Huang J, Xu S, Zou Z, Yu Y. 2023. UFL1
587 promotes antiviral immune response by maintaining STING stability independent of
588 UFMylation. Cell Death Differ 30:16-26.

589 53. Horner SM, Wilkins C, Badil S, Iskarpatyoti J, Gale M, Jr. 2015. Proteomic analysis of
590 mitochondrial-associated ER membranes (MAM) during RNA virus infection reveals
591 dynamic changes in protein and organelle trafficking. PLoS One 10:e0117963.

592 54. Zhou J, Liang Q, Dong M, Ma X, Jin Y, Guan D, Liu J, Wang M, Cong YS. 2022.
593 Optimized protocol to detect protein UFMylation in cells and in vitro via immunoblotting.
594 STAR Protoc 3:101074.

595 55. Abdelkader EH, Otting G. 2021. NT*-HRV3CP: An optimized construct of human
596 rhinovirus 14 3C protease for high-yield expression and fast affinity-tag cleavage. J
597 Biotechnol 325:145-151.

598 56. Cantell K, Hirvonen S, Kauppinen HL, Myllyla G. 1981. Production of interferon in
599 human leukocytes from normal donors with the use of Sendai virus. Methods Enzymol
600 78:29-38.

601 57. Sumpter R, Jr., Loo YM, Foy E, Li K, Yoneyama M, Fujita T, Lemon SM, Gale M, Jr.
602 2005. Regulating intracellular antiviral defense and permissiveness to hepatitis C virus
603 RNA replication through a cellular RNA helicase, RIG-I. J Virol 79:2689-99.

604 58. Fan K, Zhu K, Wang J, Ni X, Shen S, Gong Z, Cheng X, Zhang C, Liu H, Suo T, Ni X,
605 Liu H. 2022. Inhibition of 14-3-3epsilon by K50 acetylation activates YAP1 to promote
606 cholangiocarcinoma growth. Exp Cell Res 421:113404.

607 59. Hendriks IA, Lyon D, Young C, Jensen LJ, Vertegaal AC, Nielsen ML. 2017. Site-
608 specific mapping of the human SUMO proteome reveals co-modification with
609 phosphorylation. Nat Struct Mol Biol 24:325-336.

610 60. Gokhale NS, Sam RK, Somfleth K, Thompson MG, Marciniak DM, Smith JR, Genoyer E,
611 Eggenberger J, Chu LH, Park M, Dvorkin S, Oberst A, Horner SM, Ong SE, Gale M, Jr.,
612 Savan R. 2024. Cellular RNA interacts with MAVS to promote antiviral signaling.
613 Science 386:eadl0429.

614 61. Fredericksen B, Akkaraju GR, Foy E, Wang C, Pflugheber J, Chen ZJ, Gale M, Jr. 2002.
615 Activation of the interferon-beta promoter during hepatitis C virus RNA replication. Viral
616 Immunol 15:29-40.

617 62. Saito T, Hirai R, Loo YM, Owen D, Johnson CL, Sinha SC, Akira S, Fujita T, Gale M, Jr.
618 2007. Regulation of innate antiviral defenses through a shared repressor domain in RIG-
619 I and LGP2. Proc Natl Acad Sci U S A 104:582-7.
620